Journal of Materials Chemistry B

ROYAL SOCIETY OF CHEMISTRY

PAPER

View Article Online
View Journal | View Issue

Cite this: J. Mater. Chem. B, 2023, 11, 10873

Towards molecularly imprinted polymers that respond to and capture phosphorylated tyrosine epitopes using fluorescent bis-urea and bis-imidazolium receptors†

Evgeniia Kislenko, [a] Anıl İncel, [b] Kornelia Gawlitza, [a] Börje Sellergren [b] and Knut Rurack *[a]

Received 29th June 2023,
Accepted 16th October 2023

DOI: 10.1039/d3tb01474f

rsc.li/materials-b

Early detection of cancer is essential for successful treatment and improvement in patient prognosis. Deregulation of post-translational modifications (PTMs) of proteins, especially phosphorylation, is present in many types of cancer. Therefore, the development of materials for the rapid sensing of low abundant phosphorylated peptides in biological samples can be of great therapeutic value. In this work, we have synthesised fluorescent molecularly imprinted polymers (fMIPs) for the detection of the phosphorylated tyrosine epitope of ZAP70, a cancer biomarker. The polymers were grafted as nanometer-thin shells from functionalised submicron-sized silica particles using a reversible addition-fragmentation chain-transfer (RAFT) polymerisation. Employing the combination of fluorescent urea and intrinsically cationic bis-imidazolium receptor cross-linkers, we have developed fluorescent sensory particles, showing an imprinting factor (IF) of 5.0. The imprinted polymer can successfully distinguish between phosphorylated and non-phosphorylated tripeptides, reaching lower micromolar sensitivity in organic solvents and specifically capture unprotected peptide complements in a neutral buffer. Additionally, we have shown the importance of assessing the influence of counterions present in the MIP system on the imprinting process and final material performance. The potential drawbacks of using epitopes with protective groups, which can co-imprint with targeted functionality, are also discussed.

Introduction

Timely detection of cancer is crucial for successful treatment outcomes. Liquid biopsy, which involves analysing biomarkers in biological fluids using, for instance, immunoaffinity techniques, provides a non-invasive and convenient alternative to tissue biopsy.[1–3] Detecting abnormal post-translational modifications (PTMs) of proteins, particularly phosphorylation of tyrosine residues, holds promise for cancer diagnosis.[4–6] For example, ZAP70, a tyrosine-protein kinase, has been proposed as an important marker for early cancer detection and monitoring due to its pivotal role in phosphorylation.[7]

Due to a large number of potential PTM sites on proteins and the rapid advances in identifying potential biomarkers, molecularly imprinted polymers (MIPs) offer an alternative to genomics and immunoassays for diagnostic screening, as MIPs have advantages such as versatility, tuneable functionality, robustness, and ease of handling. MIPs are polymeric materials designed to selectively bind target molecules in specific cavities formed during polymerisation.[8–10] However, to broaden the scope of MIPs, the synthesis of new functional monomers and crosslinkers is essential for achieving successful imprinting.

While MIPs are widely employed for the capture and enrichment of phosphorylated proteins,[8] using structurally simpler templates such as phenylphosphonic acid[11–13] or derivatives of phosphorylated amino acids for imprinting,[14–16] there is a need for faster testing and improved detection methods. Currently, the number of reported MIPs for sensing phosphorylated tyrosine is limited,[17] even more so for phosphorylated peptides.[18,19] Existing methods often rely on core–shell particles with limited sensitivity or fluorescence response, utilising quantum dots in

[a] Chemical and Optical Sensing Division, Bundesanstalt für Materialforschung und -prüfung (BAM), Richard-Willstätter-Str. 11, D-12489 Berlin, Germany. E-mail: knut.rurack@bam.de
[b] Department of Biomedical Sciences, Faculty of Health and Society, Malmö University, SE-20506 Malmö, Sweden

† Electronic supplementary information (ESI) available: synthetic and experimental details, quantum chemical calculations, binding constant calculations, calculations of pK_a values and molar absorption coefficient of **fCL**, functionalised SiO_2 particles characterisation, spectroscopic properties and response behaviour of **fCL** and MIP and NIP core–shell polymer@SiO_2 particles, TEM images analysis for SiO_2 core particles and MIP and NIP core–shell polymer@SiO_2 particles, calculation of **fCL** amount in polymer shell of MIP and NIP core–shell polymer@SiO_2 particles, LOB, LOD and LOQ calculations and calculations of relative measurement uncertainties. See DOI: https://doi.org/10.1039/d3tb01474f

the core and analyte binding in a (non-fluorescent) MIP shell[17,18] or fluorescent probe monomers in the polymer shell grafted from a carrier particle core.[19,20] Organic urea and imidazolium monomers are commonly used for phosphorylated tyrosine capture in MIPs.[9,10,16,21] Urea groups form strong hydrogen bonds with phosphate anions,[22,23] while imidazolium salts act as effective anion receptors, interacting through electrostatic and/or hydrogen bond interactions.[24,25] Combining these units in a cooperative imprinting strategy can enhance MIP affinity through synergistic effects, particularly in polar media where hydrogen bond formation is challenging.[26] A cooperative approach has also been demonstrated for fluorescent MIPs (fMIPs).[27–29]

This study focuses on the development of fMIPs for detecting phosphorylated epitopes. Preliminary investigations employed a model analyte, phenylphosphoric acid (H_2PPA), to understand the interactions between the hydrogen bonding (neutral) fluorescent probe cross-linker, the dicationic assisting bis-imidazolium cross-linker and the anionic analyte/template. Moving from the model to a real analyte, a tripeptide (Y-pY-G) resembling the Y-Y-T epitope of the low-abundant phosphoprotein ZAP70[30] was selected for MIP synthesis. The epitope includes ^{493}Y, which is a highly-conserved autophosphorylation site for kinases.[30] The cooperative imprinting strategy utilised two functional cross-linkers to ensure high affinity and minimise non-specific binding. Besides transducing the relevant binding event in an analytical assay, the fluorescent indicator cross-linker continuously probed the structure of the imprinted site in which it is contained, allowing for rational optimisation. The study also explored the influence of epitope protective groups on the imprinting process and material selectivity, demonstrating the ability to discriminate between closely related phosphopeptide sequences.

Results and discussion

Synthesis of functional cross-linkers

The choice of functional monomers and cross-linkers is critical for successful imprinting. In this study, we focused on the sensing of the anionic phosphate group and selected a urea and a bis-imidazolium cross-linker as functional units. For phosphate recognition, we chose a fluorescent cross-linker **fCL** that carries a cleft-like urea binding motif integrated into a phenazine fluorophore (Scheme 1). This cross-linker has shown a strong affinity for phosphate groups and has been successfully used in previous work for imprinting protected phosphorylated tyrosine. It is ideal for binding of elongated molecules or side chains with a terminal phosphate group.[19,20] The synthesis of **fCL** followed a modified reaction reported previously (for more details, see Section S1, ESI†).[20]

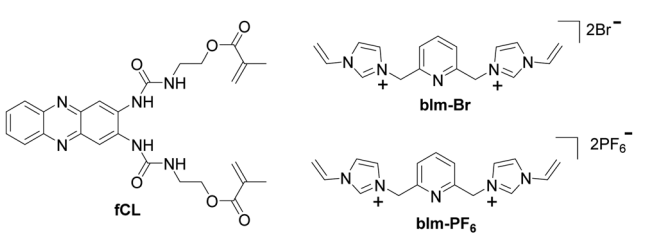

Scheme 1 Structures of functional cross-linkers used in the present work.

The bis-imidazolium salt **bIm-Br** (Scheme 1) and a related compound were previously used for synthesising MIPs for phosphate enrichment and phospholipid sensing.[16,21,31] We reasoned that the bromide anion in **bIm-Br** could potentially interact with the urea cleft of **fCL** and compete with the phosphate anion for binding sites. To overcome this unfavourable interaction and improve the solubility of bis-imidazolium cross-linkers in a non-aqueous medium, we exchanged Br^- with a weakly coordinating anion (WCA) such as hexafluorophosphate PF_6^-,[32] resulting in **bIm-PF$_6$** (Scheme 1; for more details, see Section S1, ESI†).

Pre-polymerisation studies of fCL and bIm-Br/bIm-PF$_6$

Pre-polymerisation studies were conducted to evaluate the influence of bis-imidazolium cross-linkers (**bIm-Br** or **bIm-PF$_6$**) on the complex formation between **fCL** and the template during fMIP synthesis (for more details, see Table S3 and Section S2, ESI†). Fig. 1 and Fig. S2, ESI† present the results showing the interaction between **fCL** and **bIm-Br** or **bIm-PF$_6$**. The addition of **bIm-Br** at low concentrations (0.1 eq.) induces a bathochromic shift in the absorption band of the dye, which increases with higher concentrations resulting in a 15 nm red shift for 1 eq. of **bIm-Br** (Fig. 1a and Fig. S2a, ESI†). A small red shift (5 nm) is also observed in the fluorescence emission spectra (Fig. 1b and Fig. S2b, ESI†). The fluorescence excitation spectra confirm these findings (Fig. S2c, ESI†). These observations can be explained by the formation of a complex between the bromide anion of **bIm-Br** and the urea groups of **fCL** through multiple hydrogen bonds.[33,34] The small spherical Br^- can fit inside the urea cleft of **fCL** (Fig. 1a, for more details, see Section S3, ESI†). In contrast, no bathochromic shift in absorption and emission is observed after adding **bIm-PF$_6$** to **fCL** (Fig. 1 and Fig. S2, ESI†). This can be attributed to the lower binding tendency of the hexafluorophosphate anion of **bIm-PF$_6$** to **fCL** due to its low hydrogen bond acceptor parameter[33] and steric mismatch with the urea cleft (for more details, see Section S3, ESI†).

To confirm the necessity of exchanging the bromide anion with a WCA, the competitive binding between bromide and the

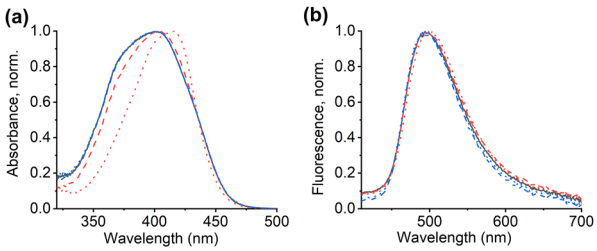

Fig. 1 Normalised absorption (a) and fluorescence emission (λ_{exc} = 385 nm) (b) spectra of pre-polymerisation mixture of **fCL** (1.11 mM) in chloroform with 0.1 eq. and 1 eq. of **bIm-Br** and **bIm-PF$_6$** in chloroform; **fCL** – black line, **fCL** and 0.1 eq. of **bIm-Br** – dashed red line, **fCL** and 1 eq. of **bIm-Br** – dotted red line, **fCL** and 0.1 eq. of **bIm-PF$_6$** – dashed blue line and **fCL** and 1 eq. of **bIm-PF$_6$** – dotted blue line.

phosphate anion was investigated, utilising phenylphosphoric acid (H_2PPA) as a model analyte.[20] When **bIm-Br** (0.1 eq.) was added to a solution of **fCL** with 1 eq. of the tetrabutylammonium (TBA) salt of $HPPA^-$ at pre-polymerisation concentrations, the bathochromic shift of 18 nm in absorption due to the formation of a hydrogen-bonded complex between the urea group and the phosphate anion remained virtually unchanged (Fig. 2a and Fig. S3a, ESI†). However, adding an equimolar amount of **bIm-Br** resulted in a slight hypsochromic shift, indicating competition between the bromide and phosphate anions for hydrogen bond formation (Fig. 2a). As both anions bind *via* hydrogen bonds, such minor effects in absorption are to be expected. A stronger influence would yet be expected in fluorescence because bromide is known to have a certain heavy-atom character, often leading to the quenching of fluorophores through the heavy atom effect.[35] Accordingly, the fluorescence response of **fCL** in the presence of template was more significantly affected by the presence of **bIm-Br**, with *ca.* 10% quenching observed upon adding 0.1 eq. of **bIm-Br** and strong quenching at equimolar concentrations, accompanied by a reversal of the initial red shift by 11 nm (Fig. 2b and Fig. S3b, ESI†). Bromide anions can thus interact with the fluorescent cross-linker **fCL** and compete with the phosphate anion for the binding sites of the fluorophore (Fig. 2), which makes the use of **bIm-Br** as a functional cross-linker in fMIP synthesis inadvisable.

In contrast, **bIm-PF$_6$** had a negligible effect on the complex formation with $HPPA^-$ (Fig. 2c, d and Fig. S4, ESI†). Based on these observations, **bIm-PF$_6$** was chosen as the cross-linker for fMIP synthesis due to its favourable characteristics and minimal interference with **fCL**-template interactions.

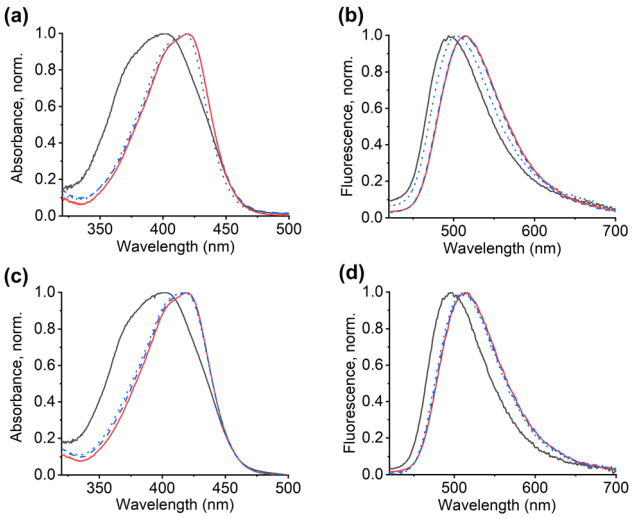

Fig. 2 Normalised absorption spectra of pre-polymerisation mixture of **fCL** (1.11 mM) in chloroform with 1 eq. of HPPA-TBA as well as 0.1 eq. and 1 eq. of **bIm-Br** (a) and (b) and **bIm-PF$_6$** (c) and (d) in chloroform; **fCL** – black line, **fCL** and 1 eq. of HPPA-TBA – red line, **fCL**, 1 eq. of HPPA-TBA and 0.1 eq. of **bIm-Br** (a) and (b) or **bIm-PF$_6$** (c) and (d) – dashed blue line and **fCL**, 1 eq. of HPPA-TBA and 1 eq. of **bIm-Br** (a) and (b) or **bIm-PF$_6$** (c) and (d) – dotted blue line.

Spectroscopic response behaviour of fCL

Prior to incorporating the functional dye **fCL** into the polymer network, its spectroscopic behaviour towards the template was reassessed considering the use of a bis-imidazolium-type co-cross-linker and chloroform as the solvent, different from our previous study, to achieve optimal binding between the two urea units and the anion.[20] The template used was the sequence Y-pY-G, which shares structural similarity with the ZAP70 epitope Y-Y-T,[36] and it was employed in its C-terminus protected form (Scheme 2a) to prevent competition with the phosphate anion for binding to the functional cross-linkers in the final MIP preparation. Additionally, the N-terminus was protected with a fluorenylmethyloxycarbonyl (Fmoc) group to enhance the solubility of the template in organic solvents. Furthermore, threonine (T) in the original epitope was replaced with glycine (G) to further improve solubility while preserving the autophosphorylation site.[30] In line with the model analyte H_2PPA, the singly deprotonated Fmoc-Y-pY-G-OMe was used for the spectroscopic experiments to ensure the formation of the hydrogen-bonded complex. TBA^+ was selected as the counter-ion as it assists in improved anion imprinting (Scheme 2a).[37]

Titrations of **fCL** in chloroform (3.14 μM) were conducted with Fmoc-Y-pY-G-OMe-TBA that interacts with **fCL** through the formation of a hydrogen-bonded complex, evidenced by a hyper- and bathochromic shift in absorption (Fig. 3a) as well as the typical red shift and enhanced fluorescence emission (Fig. 3b).[20] The binding constant was determined from the absorption spectra as $\log K_a = 4.8 \pm 0.1$ using a 1 : 1 binding model and the BindFit software (for more details, see Section S4, ESI†).[38–40] To ensure sufficient complexation of the target analyte, affinity constants $>10^3$ M^{-1} are required for stochiometric imprinting.[41] The obtained binding constants for **fCL** with Fmoc-Y-pY-G-OMe-TBA were satisfactory in this regard, enabling the synthesis of the fMIPs.

Synthesis and functionalisation of silica core particles

As highlighted in the introduction, the core–shell particle format, consisting of a carrier particle (core) and a responsive layer (shell), is particularly suitable for analytical applications involving both the capture and detection of an analyte. Accordingly, in this study, a thin MIP shell was grafted from submicron-sized silica (SiO_2) particles. Thin polymer shells offer rapid diffusion of the analyte from the surrounding medium into the MIP, which is crucial for sensing applications. Additionally, they provide binding cavities that are more homogenous and closer to the surface compared to those of monolithic polymers.

SiO_2 particles were chosen as the core particles, synthesised through a modified Stöber procedure,[42] resulting in high monodispersity. These particles could be functionalised in a straightforward manner using silane chemistry, facilitating subsequent shell growth *via* controlled living reversible addition-fragmentation chain-transfer (RAFT) polymerisation, a preferred method for such architectures.[20,43]

The SiO_2 particles prepared here had an average diameter of 318 ± 24 nm (see Fig. S10 and Section S5, ESI† for more details). They were functionalised through two condensation

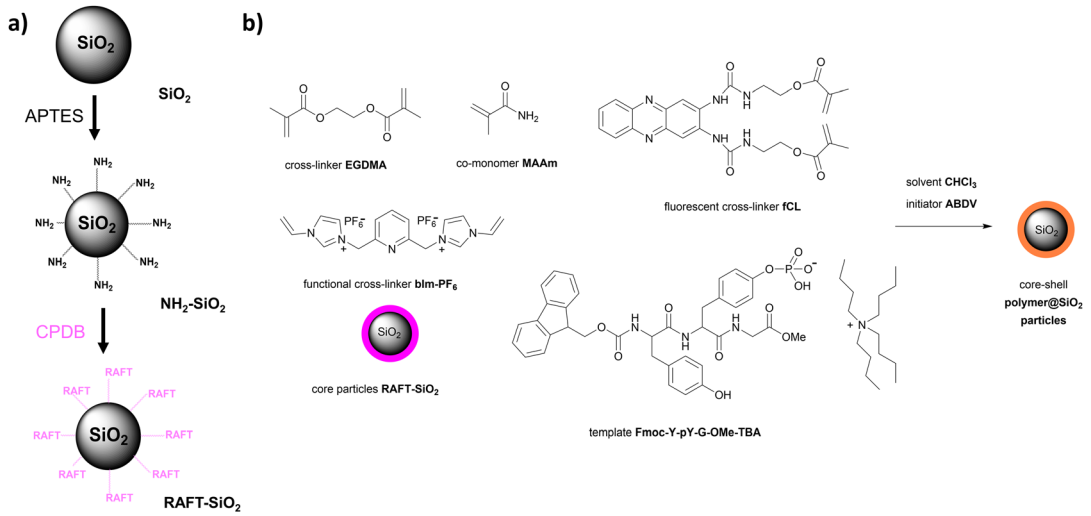

Scheme 2 (a) MIP and NIP core–shell polymer@SiO_2 particles synthesis and (b) functionalisation of SiO_2 core particles.

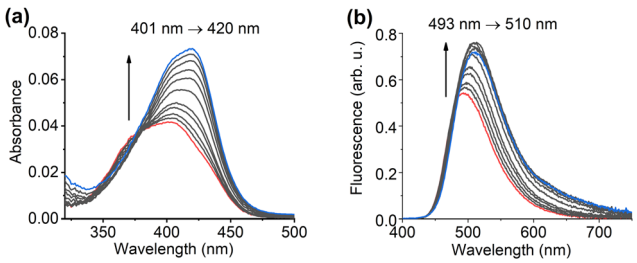

Fig. 3 Absorption (a) and fluorescence emission (λ_{exc} = 385 nm) (b) spectra of **fCL** (3.14 μM) in chloroform upon addition of an increasing amount of Fmoc-Y-pY-G-OMe-TBA (0–63.1 eq.) in chloroform; **fCL** – red line, **fCL** and 63.1 eq. of Fmoc-Y-pY-G-OMe-TBA – blue line.

reactions with amino groups using (3-aminopropyl)triethoxysilane (APTES) and the RAFT agent 4-cyano-4-(phenylcarbonothioylthio)pentanoic acid (CPDB), resulting in the formation of RAFT-SiO_2 particles (Scheme 2b). Detailed synthetic and characterisation information can be found in Sections S1, S5 and S6, ESI.†

The successful functionalisation of the particles was confirmed through zeta potential measurements, thermogravimetric analysis (TGA) and elemental analysis; see Fig. S13 and Section S6 for more details, ESI.†

MIP and NIP core–shell polymer@SiO_2 particles synthesis

After preliminary experiments, fluorescent core–shell polymer@SiO_2 MIP and NIP particles were synthesised for the detection of the Y-pY-G sequence, structurally similar to the ZAP70 epitope Y-Y-T.[30,36] The synthesis involved the use of the fluorescent cross-linker **fCL**, the template Fmoc-Y-pY-G-OMe-TBA, the structural cross-linker ethylene glycol dimethacrylate (EGDMA), the structural co-monomer methacrylamide (MAAm) and the functional cross-linker **bIm-PF_6** (Scheme 2a).

EGDMA, a hydrophilic cross-linker, was employed to achieve highly cross-linked and rigid shells during polymerisation, promoting the formation of specific binding cavities for improved analyte recognition. It was used in excess compared to the functional cross-linkers as well as the template to ensure effective cross-linking. MAAm, a neutral co-monomer, was included based on its demonstrated enhancement of the imprinting process in similar MIP systems.[20] The deprotonated phosphate group in Fmoc-Y-pY-G-OMe-TBA could form the desired hydrogen-bonded complex with both urea moieties of fluorophore **fCL** and the H2 protons of **bIm-PF_6** (see Fig. S1, ESI†). Furthermore, the presence of positive charges in **bIm-PF_6** could enhance imprinting by replacing the TBA cation as the counterion in the ternary ensemble of **fCL**:template anion:counter-cation.

It is important to note that unlike the displacement of the template to a minor extent by Bis-Im^{2+}, the exchange of a TBA counterion with Bis-Im^{2+} would not hinder imprinting but could instead result in more rigid cavities, as the Bis-Im^{2+} counterion would be fixed in the network alongside the [**fCL**⊂pY(R_1R_2)]$^-$/Bis-Im^{2+}/PF_6^- complex (see discussion below and Section S12, ESI†). Therefore, employing both functional cross-linkers simultaneously during MIP synthesis has the potential to yield more precisely tailored cavities and enhance the analytical response.

To investigate the impact of polymer network composition on imprinting, two batches of particles with different monomer concentrations (**M1bIm** and **M2bIm**) were synthesised (Table 1). **M1bIm** was produced using lower amounts of polymerisation components and a higher quantity of initiator, while **M2bIm** was prepared with a higher monomer concentration and a lower amount of initiator. To ensure complete solubilisation of the functional cross-linkers in chloroform and prevent dimerization, the concentrations of **fCL** and **bIm-PF_6** were kept low. A stochiometric imprinting ratio of 1 : 0.5 : 1 (**fCL** : **bIm-PF_6** : template) was maintained to ensure precise and effective imprinting.[41]

As control materials, non-imprinted polymers (NIPs), referred to as **N1bIm** and **N2bIm**, were synthesised simultaneously using a procedure identical to MIP preparation but without adding the

Table 1 Amount of polymerisation components for **M1bIm**, **N1bIm**, **M2bIm** and **N2bIm** core–shell polymer@SiO_2 particles

Sample	Fmoc-Y-pY-*G*-OMe (mg)	**fCL** (mg)	MAAm (mg)	**bIm-PF$_6$** (mg)	EGDMA (μL)	ABDV (mg)	$CHCl_3$ (mL)	RAFT-SiO_2 (mg)
M1bIm	1.01	0.55	1.83	0.31	20.6	2	2	20
N1bIm	—	0.55	1.83	0.31	20.6	2	2	20
M2bIm	2.8	1.52	5.06	0.85	56.12	0.78	2	20
N2bIm	—	1.52	5.06	0.85	56.12	0.78	2	20

analyte. The pre-polymerisation mixtures for both MIP and NIP batches were sampled directly from the polymerisation reaction prior to the addition of the initiator and particles. This allowed for examining the influence of cross-linkers and co-monomers and assessing the stability of the complex between the template and fluorescent probe **fCL**.

Lower monomer and **fCL** concentrations in the pre-polymerisation mixtures of **M1bIm** and **N1bIm** resulted in reduced absorption and fluorescence intensities compared with **M2bIm** and **N2bIm**. Absorption and fluorescence spectra of **N1bIm** particles (Fig. S14a and c, ESI†) were similar to the free dye but slightly red-shifted compared to diluted conditions (Fig. 3). Similar spectra were observed for **N2bIm** (Fig. S14b and d, ESI†). Upon template addition, both batches exhibited a red shift and intensity increase in absorption and fluorescence (Fig. S14, ESI†), indicating the successful formation of the complex between **fCL** and Fmoc-Y-pY-G-OMe-TBA. The red shift in the pre-polymerisation mixture with an equimolar amount of template was similar to diluted conditions (*cf.* Fig. 3 *vs.* Fig. S14, ESI†). Although a higher enhancement was observed for **M1bIm** compared to **N1bIm**, **M2bIm** showed a more pronounced red shift than **N2bIm** (Fig. S14, ESI†). However, the intensity effect may be only apparent, possibly due to different changes in absorbance at the excitation wavelength that could not be measured under the present conditions.

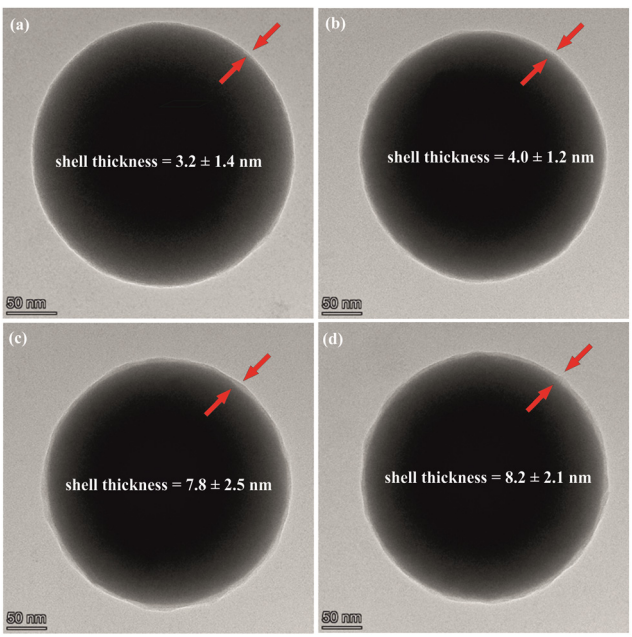

Fig. 4 TEM images of **M1bIm** (a), **N1bIm** (b), **M2bIm** (c) and **N2bIm** (d) core–shell polymer@SiO_2 particles. Scale bar = 50 nm.

Following the synthesis and washing of the core–shell polymer@SiO_2 particles, the formation of the polymer network was evaluated using TEM (Fig. 4; Table S4 and Section S5, ESI†). All core–shell polymer@SiO_2 particles exhibit an even shell, indicating successful polymerisation. The MIP shell thickness (Fig. 4a and c) was slightly lower and more polydisperse compared to the corresponding NIPs (Fig. 4b and d). The presence of the template may influence the reactivity rates of the monomers and co-monomers due to hydrogen bonding and/or electrostatic interaction.[44] **M1bIm** and **N1bIm** (Fig. 4a and b) had thinner shells than the second particle batch (Fig. 4c and d), reflecting the difference in initial monomer and initiator concentrations. The successful removal of the template was also confirmed by absorption measurements of MIP and NIP suspensions at identical concentrations of 0.5 mg mL^{-1} in chloroform, which yielded identical spectra (Fig. S15, ESI†). The concentration of the dye in the polymer layer was estimated using the absorption spectra of MIP and NIP suspensions and the molar absorption coefficient of fluorophore **fCL** in chloroform at 401 nm of ε_{401} = 13 638 ± 573 M^{-1} cm^{-1} (for more details, see Sections S8 and S9, ESI†). The results showed that MIP particles incorporated a lower amount of **fCL** compared to non-imprinted particles, supporting the idea that the polymerisation rate depends on the presence of the template and is influenced by the complexation process between monomers and template (Table S5, ESI†).[44] The concentration of the dye in the polymer shells was comparable for both MIPs and both NIPs, indicating that changing the polymerisation ingredients influenced the shell thickness but not the dye concentration.

Analytical performance of MIP and NIP particles in chloroform

To evaluate the response of the MIP particles, titration experiments were conducted using the same solvent as the one used for polymerisation to ensure that the polymer shell's swelling behaviour remained unaltered, and all the imprinted sites were accessible for analyte rebinding. Absorption and fluorescence spectra were measured upon the addition of Fmoc-Y-pY-G-OMe-TBA in chloroform at a particle concentration of 0.5 mg mL^{-1} (Fig. 5).

The binding affinity of Fmoc-Y-pY-G-OMe-TBA to the **M1bIm** and **M2bIm** core–shell polymer@SiO_2 particles was evaluated using the corrected absorption spectra (Fig. S19, ESI†). Binding constants of $\log K_a$ = 5.4 ± 0.3 and 5.4 ± 0.2 for **M1bIm** and **M2bIm**, respectively, were calculated using a 1 : 1 binding model (Fig. S20, ESI†). The binding constants were higher compared to the interaction of **fCL** and the tripeptide epitope

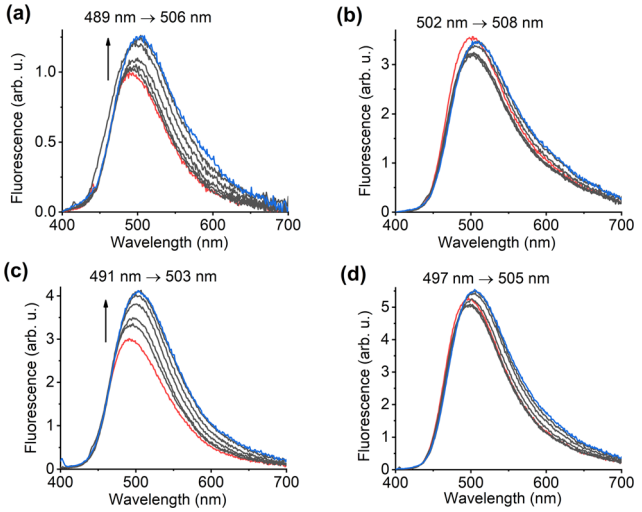

Fig. 5 Fluorescence emission (λ_{exc} = 385 nm) spectra of **M1bIm** (a), **N1bIm** (b), **M2bIm** (c) and **N2bIm** (d) core–shell polymer@SiO_2 particles (0.5 mg mL^{-1}) in chloroform upon addition of an increasing amount of Fmoc-Y-pY-G-OMe-TBA (0–69.8 μM) in chloroform; **M1bIm**, **N1bIm**, **M2bIm** and **N2bIm** – red line, **M1bIm**, **N1bIm**, **M2bIm** and **N2bIm** and 69.8 μM of Fmoc-Y-pY-G-OMe-TBA – blue line.

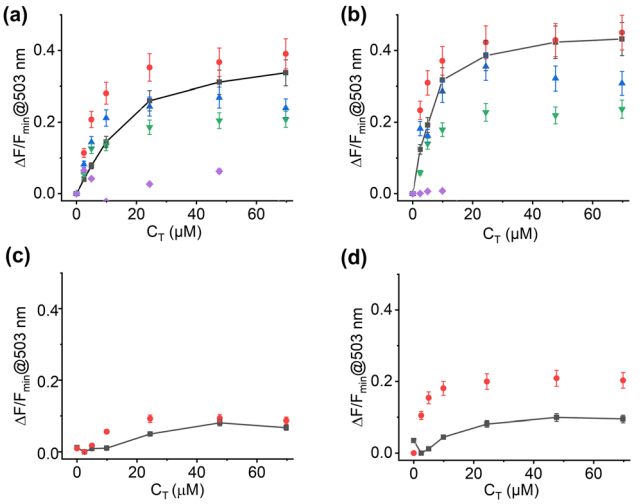

Fig. 6 Relative fluorescence emission (λ_{exc} = 385 nm) intensity change at λ = 503 nm for **M1bIm** (a), **M2bIm** (b), **N1bIm** (c) and **N2bIm** (d) core–shell polymer@SiO_2 particles (0.5 mg mL^{-1}) in chloroform upon addition of an increasing amount of analytes (0–69.8 μM) in chloroform; Fmoc-Y-pY-G-OMe-TBA – black ■ with line, Fmoc-pY-OEt-TBA – red ●, HPPA-TBA – blue ▲, HPPA-THA – green ▼ and Fmoc-Y-Y-G-OMe – purple ♦. Measurement uncertainties as indicated for selected data points. $\Delta F/F_{min}$ = $(F_x - F_{min})/F_{min}$. C_T – concentration of template.

in a diluted state ($\log K_a = 4.8 \pm 0.1$), indicating an increase in the affinity of the analyte towards the integrated **fCL** in the polymer network.

During the titration, a red shift of *ca.* 10 nm and an enhancement in fluorescence emission were observed upon template addition to the MIP particles. The intensity reached saturation at *ca.* 70 μM of the analyte (Fig. 5a and c). The fluorescence response was similar for both MIPs, indicating comparable accessibility of **fCL** to the template despite the different shell thicknesses. The bathochromic shift was smaller compared to dilute conditions, which can be explained by the presence of a highly cross-linked polymer network in which it is more difficult to achieve a fully relaxed conformation and an optimal arrangement of **fCL** and Fmoc-Y-pY-G-OMe-TBA.

The fluorescence response of the NIP particles to template addition was considerably smaller, indicating a highly cross-linked network with no specific binding sites for the template (Fig. 5b and d). The fluorescence change in NIP particles may be attributed to non-specific interaction between the analyte and the dye in the outer polymer shell. The fluorescence emission spectra of **N1bIm** and **N2bIm** were red shifted compared to the corresponding imprinted particles (Fig. 5). This may be due to an even denser polymer network, which, because the structural monomer and cross-linker are more polar than chloroform, may lead to better dipolar stabilisation of an excited charge-transfer state, as it is the relevant emitting state in **fCL**.[45]

The fluorescence intensity enhancement of both MIPs was higher compared to the corresponding NIPs (*cf.* Fig. 6a, b *vs.* c and d). The imprinting factor (IF), calculated as the ratio of intensity change between MIP and NIP at the maxima of the fluorescence band, was 5.0 and 4.5 for **M1bIm** and **M2bIm**, respectively (Fig. 6). The limit of detection for **M1bIm** was determined to 11.2 μM (for more details, see Section S15, ESI†).

To assess the discrimination factor (DF) between the targeted analyte and competitor molecules, titrations were performed using Fmoc-Y-Y-G-OMe as a related compound and competitors, including Fmoc-pY-OEt-TBA, HPPA-TBA and HPPA-THA (Scheme 3). **M1bIm** and **M2bIm** exhibited minimal response when titrated with Fmoc-Y-Y-G-OMe, which agrees well with the absence of a response upon titration of fCL with the competitor (Fig. 6a, b and Fig. S22e, f, *cf.* Fig. S23, ESI†).

Both **M1bIm** and **M2bIm** show no discrimination between the targeted tripeptide and Fmoc-protected phosphorylated

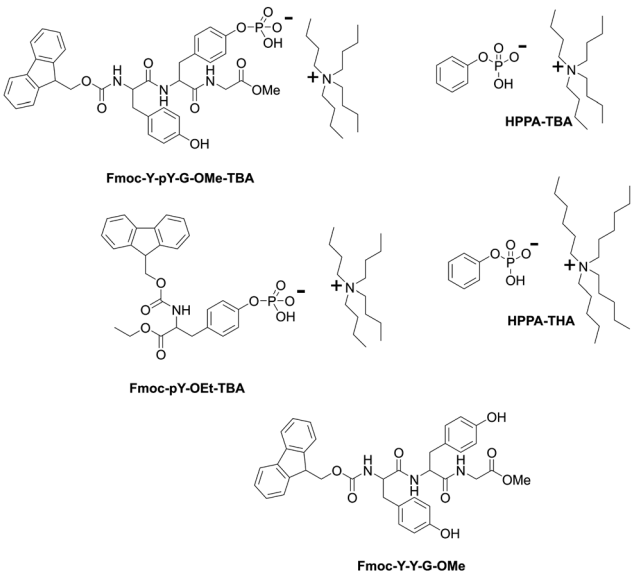

Scheme 3 Structures of target analyte and related molecules.

tyrosine (Fig. 6a, b and Fig. S24, ESI†), suggesting that the presence of the Fmoc protective group, which is imprinted during polymerisation, plays a role in inducing a similar or slightly stronger response. Comparison with the non-imprinted control materials confirmed that the smaller protected amino acid molecule could more easily diffuse into the highly cross-linked polymer shell and may more easily adopt an optimum fit into the cleft, inducing a slightly enhanced response (Fig. 6c, d and Fig. S24, ESI†).

Further titration of **M1bIm** and **M2bIm** with HPPA-TBA, a competitor molecule, resulted in a weaker response compared to Fmoc-Y-pY-G-OMe-TBA or Fmoc-pY-OEt-TBA, with a DF of *ca.* 1.4 for both **M1bIm** and **M2bIm** (Fig. 6a, b and Fig. S22, ESI†). The difference may be attributed to the absence of the Fmoc group in HPPA-TBA. However, when the bulkier tetrahexylammonium salt of $HPPA^-$ (HPPA-THA) was employed, more pronounced discrimination factors of 1.6 and 1.8 for **M1bIm** and **M2bIm**, respectively, were observed (Fig. 6a and b). This stresses the conclusion that additional π–π stacking interactions with the Fmoc group enhance the binding of protected amino acid and peptide species and that the presence of longer hydrophobic alkyl chains of counterions further prevents such interactions.[37]

From the cross-selectivity studies, it can be concluded that a stronger response of the imprinted material can be achieved if the analyte has a high number of aromatic moieties. Complementary π–π interactions together with hydrogen bonds and electrostatic interactions may be responsible for the binding of the analyte to the polymer network.[46] These results for the **M1** and **M2** systems also showed that the behaviour is virtually independent of the synthetic method used, which underlines the robustness of the approach.

To further investigate the impact of the synthesised bis-imidazolium cross-linker in the polymer network on the behaviour of imprinted materials, two additional batches of imprinted polymers were prepared with slight modifications to the **M1bIm** and **N1bIm** recipes (Table S1, ESI†). The first batch (**M1no**, **N1no**) was synthesised without **bIm-PF_6** to evaluate the effect of a cooperative imprinting strategy on material performance. The second batch (**M1D**, **N1D**) replaced **bIm-PF_6** with an equivalent amount of divinylbenzene (DVB-80) cross-linker to assess the impact of increased cross-linking and more sites for π–π stacking on the MIP's affinity towards Fmoc-Y-pY-G-OMe-TBA, without the presence of synergistic interactions between functional monomers. Compared to **M1bIm**, both batches showed significantly lower imprinting factors (IF) (1.4 for **M1no**, 2.2 for **M1D**, see Fig. S26, ESI† for a comparison). This suggests that the higher affinity of the target molecule to imprinted materials, as compared to NIPs, cannot be solely attributed to the formation of tighter binding cavities in the dense polymer network. Our findings highlight the advantages of employing complementary imprinting using **fCL** and **bIm-PF_6** (for more details, see Section S12, ESI†).

Analytical performance of MIP and NIP particles in aqueous buffer

For the detection of oxoanions using organic molecular probes, fluorescence signalling relies on hydrogen bonding interaction typically occurring in a classical supramolecular chemistry sense *via* two hydrogen bonding partners in a low-dielectric microenvironment. However, for more challenging analytes such as sugar acids, glycosylated amino acids or peptides, which are present in a multicomponent network along with the indicator molecule, alternative signalling modes can become active, as shown above, and in ref. 28,29, making such approaches potentially useful for aqueous media where hydrogen bond-driven fluorescence signalling is not feasible.

To evaluate the capability of the MIPs to capture the imprinted template in aqueous buffers, resembling real-life conditions for detecting phosphoproteins in cell lysates, we performed a four-fold scale-up synthesis of **M1bIm** and **N1bIm**, resulting in **M3bIm** and **N3bIm**, respectively (Table S2, ESI†). Characterisation confirmed the reproducibility of the synthesis, see, *e.g.*, Table S4 and Fig. S10, ESI.† Furthermore, we obtained three decapeptides representing the ZAP70 kinase regulatory motif (Scheme S5, ESI†) and dissolved them in aqueous buffers of various pH values (from 1.0–9.2), corresponding to the operating range of **fCL** in its neutral form (Section S14, ESI†). Equilibrium binding tests were conducted by incubating **M3bIm** and **N3bIm** with the peptide mixtures, followed by quantification of unbound peptides using reverse phase HPLC with UV detection.

Fig. 7 illustrates the percentage binding of the different peptides to the MIPs and NIPs. In the low pH region (pH 1–5), it is evident that peptide uptake does not strongly correlate with the desired selectivity (YpY). Instead, binding appears to be influenced by the ionisation degree, as observed by the significant increase in binding of the multiply phosphorylated target when the buffer pH is increased from 3 to 5. This can be explained by examining the net charges of the peptides, where the charge of pYpY changes from −1 to −3 within this range (Table 2).

Of particular interest is the binding behaviour in neutral buffer conditions. MIPs exhibit preferential uptake of the phosphopeptide complement, with YpY binding more strongly than pYpY and YY (Fig. 7a). In contrast, NIPs show no such selectivity (Fig. 7b). The higher non-specific binding of the NIPs could be mitigated by employing ''dummy NIPs'', as demonstrated in previous studies, which yield more realistic control

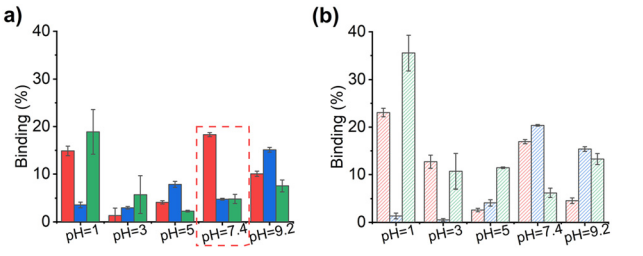

Fig. 7 Binding of **M3bIm** (a) and **N3bIm** (b) core–shell polymer@SiO_2 particles (10 mg mL^{-1}) after incubation in decapeptides mixture of GADDSY**pY**TAR, GADDS**pYpY**TAR and GADDS**YY**TAR (20 μM) in aqueous buffers; **M3bIm** binding – solid bar, **N3bIm** binding – shaded bar, GADDSYpYTAR percentage bound – red, GADDSpYpYTAR percentage bound – blue and GADDSYYTAR percentage bound – green.

Table 2 Net charge of decapeptides at the differently buffered pH employed here

pH	GADDSYYTAR	GADDSYpYTAR	GADDSpYpYTAR
1	2	2	2
3	1	0	−1
5	−1	−2	−3
7.4	−1	−3	−5
9.2	−1	−3	−5

polymers for highly hydrophilic biomolecule targets.[28] In this case, the increased non-specific binding may result from hydrophobic interactions and the presence of **bIm-PF$_6$** cross-linkers that are more randomly distributed throughout the network, offering cationic sites for non-specific interactions.

To interpret these findings in aqueous media at varying pH, it is important to understand the relationship between fluorescence assays in organic media and the capture data obtained by HPLC in aqueous media. Weaker (and different) or no fluorescence signalling would be expected in highly polar or protic environments, but binding within the cavities can still occur, similar to conventional non-fluorescent MIPs. The intention of testing the system in aqueous media was not to replicate the fluorescence response but rather to assess whether the discrimination observed in the polymerisation solvent is maintained in an analytically important pH range in water, particularly near-neutral pH. The step from chloroform to buffered aqueous media involves different swelling behaviour, electrolyte content, ionic components of the buffer, and charge states of the analytes. As the charge state of the analyte significantly influences its conformational structure, our goal was to minimise the factors influencing the system and determine if the binding pattern remains comparable to the fluorescence assay in near-neutral pH conditions relevant to sensing in diluted biological fluids. A comparison of the data in Fig. 6 and 7 confirms that this is indeed the case.

Contrary to intuition, we did not expect the polymers to maintain the binding pattern over a wide pH range (pH 1.0–9.2), where the charge states of the species vary between +1 and −5 (Table 2). These charge states affect peptide conformation and the presence of counterions in close proximity to the charged groups. It would be unlikely for a MIP with selective binding pockets to accommodate a wide range of species with different conformations, charges, and counterions. Therefore, it is expected that discriminative binding would be observed within a narrow but relevant pH window, as observed in the present case.

Fluorescence measurements performed on this system in differently buffered solutions did not reveal clear fluorescence changes, which was anticipated because, as explained in the beginning of this section, the present signalling mode is solely based on hydrogen bond interactions which are too inefficient for the present system. However, the favourable binding behaviour at neutral pH is encouraging for the development of fluorescent indicator monomers and cross-linkers. Once a more suitable fluorescent monomer or cross-linker capable of responding to the target phosphate group in water is identified, possibly also involving alternative signalling modes, its incorporation into the present MIP system holds promise for creating an fMIP system capable of binding and sensing in water.

Conclusions

We have developed a fluorescent molecularly imprinted polymer (fMIP) capable of distinguishing phosphorylated and non-phosphorylated epitopes of ZAP70. Our study demonstrated that cooperative imprinting using a colourless and non-fluorescent bis-imidazolium cross-linker improves the generation of imprinted cavities compared to using a fluorescent urea cross-linker alone. Including counterions in the imprinting models enhances the evaluation and prediction of MIP performance. By utilising complementary and cooperative interactions, bulky polar anions can be effectively imprinted into the organic polymer, as observed in fluorescence rebinding studies. However, imprinting protected epitopes may decrease selectivity towards target analytes due to the co-imprinting of protective groups. Nevertheless, when assessing peptide recognition in aqueous systems at neutral pH, we obtained favourable results with remarkable peptide specificity that aligned with the intended selectivity. Despite the challenges involved in transferring the MIP system from an organic to an aqueous environment, these findings suggest that our imprinting strategy is robust and holds great promise for developing fluorescent indicator-containing MIPs capable of binding and indicating target analytes under realistic conditions. The synthesised particles can potentially be integrated into microfluidic devices for the rapid detection of cancer biomarkers,[19] such as small-number amino acid peptides, by transferring them from an aqueous sample to an organic signalling phase. Ongoing research in our laboratories focuses on both the development of indicator monomers/cross-linkers and the advancement of microfluidic assay platforms.

Experimental

Synthesis of M1bIm, N1bIm, M2bIm and N2bIm core–shell polymer@SiO$_2$ particles

MIP and NIP layers were grafted from the RAFT-SiO$_2$ particles using two different recipes (Table 1). EGDMA was purified by passing through a Pasteur pipette containing inhibitor remover for hydroquinone and monomethyl ether hydroquinone. MAAm was used without additional purification. A 2 mM stock solution of freshly prepared Fmoc-Y-pY-G-OMe-TBA (for more details, see Section S1, ESI†) was prepared by dissolving in anhydrous chloroform and briefly sonicated. **bIm-PF$_6$** (0.31 mg, 0.53 μmol for **M1bIm** and **N1bIm** or 0.85 mg, 1.46 μmol for **M2bIm** and **N2bIm**), MAAm (1.83 mg, 21.07 μmol for **M1bIm** and **N1bIm** or 5.06 mg, 58.32 μmol for **M2bIm** and **N2bIm**), EGDMA (20.6 μL, 105.37 μmol for **M1bIm** and **N1bIm** or 56.12 μL, 291.62 μmol for **M2bIm** and **N2bIm**), and fluorescent cross-linker **fCL** (0.55 mg, 1.05 μmol for **M1bIm** and **N1bIm** or 1.52 mg, 2.92 μmol for **M2bIm** and **N2bIm**) were combined in specific amounts according to the recipes. In the MIP vial, the

template solution (0.53 mL for **M1bIm** or 1.46 mL for **M2bIm**) and chloroform (1.47 mL for **M1bIm** or 0.54 mL for **M2bIm**) were added, while only chloroform (2 mL) was added to the NIP vials. The solutions were sonicated for 10 min. A small portion of the reaction solution (30 μL) was used for control purposes in prepolymerisation studies. RAFT-SiO_2 particles (20 mg) were then added, and the suspensions were sonicated for another 10 min. Under argon, the initiator ABDV (2 mg for **M1bIm** and **N1bIm** or 0.79 mg for **M2bIm** and **N2bIm**) was added to the reaction mixture. The mixture was cooled, degassed with argon for 5 min, and then mixed at moderate speed in a hybridisation oven at 50 °C. After 16 h, the temperature was increased to 70 °C. After an additional 2 h, the particles were precipitated using n-hexane (4 mL), washed with chloroform (2 mL) and acetonitrile (2× 4 mL and 2× 1.8 mL) with centrifugation at 6500 ×*g* for 5 min and 4800 ×*g* for 10 min in between the washing steps. The particles were incubated for 1 h in methanol/acetic acid 9 : 1 solution (3× 1.8 mL) using a rotator (40 rpm), followed by sonication (10 min) and centrifugation (4800 ×*g*, 10 min). The particles were additionally washed with methanol (2× 1.8 mL), sonicated, and centrifuged (4800 ×*g*, 10 min) before drying overnight in a vacuum oven.

Titrations of particles

The fluorescence response of MIP and NIP core–shell polymer@SiO_2 particles to analyte addition was evaluated in 10 × 10 mm quartz cuvettes. The particles were suspended in chloroform (0.5 mg mL^{-1}) and sonicated for 15 min prior to measurement. A freshly prepared analyte stock solution (1 mM) was used. Before each measurement, the suspension was equilibrated for 2 min using a magnetic stirring bar and a motorised cuvette holder. Fluorescence measurements were conducted with an excitation wavelength of 385 nm, and fluorescence excitation spectra were recorded at an emission wavelength of 490 nm. Slits were adjusted to keep the signal intensity below 10^6 counts per second.

Imprinting factor (IF) and discrimination factor (DF)

IF, the imprinting factor, can be determined by calculating the ratio of fluorescence intensity change between MIP and NIP core–shell polymer@SiO_2 particles. This is expressed in eqn (1), where F_x represents the emission intensity at λ = 503 nm of a particle suspension upon reaching signal saturation with the template/analyte, and F_{min} represents the emission intensity at λ = 503 nm of a particle suspension in the absence of a template:

$$\begin{aligned} \mathrm{IF} &= \left(\frac{F_x - F_{min}}{F_{min}}\right)_{MIP} \Big/ \left(\frac{F_x - F_{min}}{F_{min}}\right)_{NIP} \\ &= \left(\frac{\Delta F}{F_{min}}\right)_{MIP} \Big/ \left(\frac{\Delta F}{F_{min}}\right)_{NIP} \end{aligned} \quad (1)$$

DF, the discrimination factor, can be calculated as the ratio of intensity change in MIP core–shell polymer@SiO_2 particles upon the addition of the template and a competitor molecule. This is shown in eqn (2), where ΔF represents F_x–F_{min} of Eqn 1 after achieving signal saturation with the analyte as well as the competitor, and F_{min} represents the emission intensity at λ = 503 nm of a particle suspension in the absence of a guest:

$$\mathrm{DF} = \left(\frac{\Delta F}{F_{min}}\right)_{\substack{\mathrm{MIP} \\ \text{with analyte}}} \Big/ \left(\frac{\Delta F}{F_{min}}\right)_{\substack{\mathrm{MIP} \\ \text{with competitor}}} \quad (2)$$

Capture studies in aqueous buffers

To assess the binding of MIP and NIP core–shell polymer@SiO_2 particles, a 20 μM solution (C_0) of three decapeptides (GADDSYpYTAR (YpY) + GADDSpYpYTAR (pYpY) + GADDSYYTAR (YY)) in aqueous buffers with pH values of 1.0, 3.0, 5.0, 7.4, 9.2, were prepared. The particles were suspended in a peptide mixture (10 mg mL^{-1}) and sonicated for 15 min. Following vigorous shaking during a 2 h incubation, centrifugation at 14 000 × *g* for 15 min was performed. The resulting supernatant was collected, concentrated using a Genevac EZ-2 evaporator, and reconstituted in a water/acetonitrile 95 : 5 v/v solution containing 0.1% trifluoroacetic acid. The peptide concentrations were determined using HPLC (n = 3). The binding of the polymer was calculated using eqn (3), where C_{free} represents the concentration of peptide in the supernatant, and C_0 represents the concentration of peptide in the peptide mixture:

$$B = \frac{C_{free}}{C_0} \times 100\% \quad (3)$$

Conflicts of interest

There are no conflicts to declare.

Acknowledgements

We thank M. Grüneberg (BAM) for TGA measurements and synthetic support, K. Keil (BAM) for SiO_2 particle synthesis, zeta potential and pK_a measurements, V. Perez Padilla (BAM) for experimental support, B. Kobin (Humboldt University Berlin, HUB) for MS analysis, J. Krone (TU Berlin) and A. Meckelburg (BAM) for performing elemental analyses, and A. Zimathies (BAM) for N_2 adsorption/desorption measurements. This work has received funding from the European Union's Horizon 2020 research and innovation programme under the Marie Skłodowska-Curie grant agreement no. 722171.

Notes and references

1 R. Vaidyanathan, R. H. Soon, P. Zhang, K. Jiang and C. T. Lim, *Lab Chip*, 2019, **19**, 11–34.
2 P. Pinzani, V. D'Argenio, M. D. Re, C. Pellegrini, F. Cucchiara, F. Salvianti and S. Galbiati, *Clin. Chem. Lab. Med.*, 2021, **59**, 1181–1200.
3 M. Ignatiadis, G. W. Sledge and S. S. Jeffrey, *Nat. Rev. Clin. Oncol.*, 2021, **18**, 297–312.
4 V. Singh, M. Ram, R. Kumar, R. Prasad, B. K. Roy and K. K. Singh, *Protein J.*, 2017, **36**, 1–6.
5 Y. P. Lim, *Clin. Cancer Res.*, 2005, **11**, 3163–3169.

6 K. Rikova, A. Guo, Q. Zeng, A. Possemato, J. Yu, H. Haack, J. Nardone, K. Lee, C. Reeves, Y. Li, Y. Hu, Z. Tan, M. Stokes, L. Sullivan, J. Mitchell, R. Wetzel, J. MacNeill, J. M. Ren, J. Yuan, C. E. Bakalarski, J. Villen, J. M. Kornhauser, B. Smith, D. Li, X. Zhou, S. P. Gygi, T.-L. Gu, R. D. Polakiewicz, J. Rush and M. J. Comb, *Cell*, 2007, **131**, 1190–1203.
7 J. A. Orchard, R. E. Ibbotson, Z. Davis, A. Wiestner, A. Rosenwald, P. W. Thomas, T. J. Hamblin, L. M. Staudt and D. G. Oscier, *Lancet*, 2004, **363**, 105–111.
8 P. Zhang, L.-Y. Jiang, J.-T. Ma and Q. Jia, *Chin. J. Anal. Chem.*, 2021, **49**, 24–33.
9 J. Chen, S. Shinde, P. Subedi, C. Wierzbicka, B. Sellergren, S. Helling and K. Marcus, *J. Chromatogr. A*, 2016, **1471**, 45–50.
10 A. İncel, S. Shinde, I. A. Diez, M. M. Stollenwerk, O. N. Jensen and B. Sellergren, *ChemRxiv*, Cambridge: Cambridge Open Engage, 2022, DOI: **10.26434/chemrxiv-2022-bzkrq**.
11 Q. S. Li, F. Shen, X. Zhang, Y. F. Hu, Q. X. Zhang, L. Xu and X. Q. Ren, *Anal. Chim. Acta*, 2013, **795**, 82–87.
12 L. Xu, Y. F. Hu, F. Shen, Q. S. Li and X. Q. Ren, *J. Chromatogr. A*, 2013, **1293**, 85–91.
13 X. Q. Yang and Y. Xia, *J. Sep. Sci.*, 2016, **39**, 419–426.
14 M. Emgenbroich, C. Borrelli, S. Shinde, I. Lazraq, F. Vilela, A. J. Hall, J. Oxelbark, E. De Lorenzi, J. Courtois, A. Simanova, J. Verhage, K. Irgum, K. Karim and B. Sellergren, *Chem. – Eur. J.*, 2008, **14**, 9516–9529.
15 A. Incel, I. A. Diez, C. Wierzbicka, K. Gajoch, O. N. Jensen and B. Sellergren, *Anal. Chem.*, 2021, **93**, 3857–3866.
16 C. Wierzbicka, M. Liu, D. Bauer, K. Irgum and B. Sellergren, *J. Mater. Chem. B*, 2017, **5**, 953–960.
17 R. Gui and H. Jin, *J. Photochem. Photobiol., C*, 2019, **41**, 100315.
18 D. Y. Li, Y. P. Qin, H. Y. Li, X. W. He, W. Y. Li and Y. K. Zhang, *Biosens. Bioelectron.*, 2015, **66**, 224–230.
19 S. C. Burnage, J. Bell, W. Wan, E. Kislenko and K. Rurack, *Lab Chip*, 2023, **23**, 466–474.
20 W. Wan, A. B. Descalzo, S. Shinde, H. Weißhoff, G. Orellana, B. Sellergren and K. Rurack, *Chem. – Eur. J.*, 2017, **23**, 15974–15983.
21 P. Narayanaswamy, S. Shinde, R. Sulc, R. Kraut, G. Staples, C. H. Thiam, R. Grimm, B. Sellergren, F. Torta and M. R. Wenk, *Anal. Chem.*, 2014, **86**, 3043–3047.
22 V. Amendola, L. Fabbrizzi and L. Mosca, *Chem. Soc. Rev.*, 2010, **39**, 3889–3915.
23 S. Pal, T. K. Ghosh, R. Ghosh, S. Mondal and P. Ghosh, *Coord. Chem. Rev.*, 2020, **405**, 213128.
24 Y. Hu, S. Long, H. Fu, Y. She, Z. Xu and J. Yoon, *Chem. Soc. Rev.*, 2020, **50**, 589–618.
25 K. Dong, S. Zhang and J. Wang, *Chem. Commun.*, 2016, **52**, 6744–6764.
26 S. Farshbaf and P. Anzenbacher, *Chem. Commun.*, 2019, **55**, 1770–1773.
27 S. Shinde, Z. El-Schich, A. Malakpour, W. Wan, N. Dizeyi, R. Mohammadi, K. Rurack, A. Gjoerloff Wingren and B. Sellergren, *J. Am. Chem. Soc.*, 2015, **137**, 13908–13912.
28 M. Kimani, S. Beyer, Z. El-Schich, K. Gawlitza, A. Gjörloff-Wingren and K. Rurack, *ACS Appl. Polym. Mater.*, 2021, **3**, 2363–2373.
29 S. Jiang, T. Wang, S. Behren, U. Westerlind, K. Gawlitza, J. L. Persson and K. Rurack, *ACS Appl. Nano Mater.*, 2022, **5**, 17592–17605.
30 A. C. Chan, M. Iwashima, C. W. Turck and A. Weiss, *Cell*, 1992, **71**, 649–662.
31 Q. Li, T. Wang, Y. Jin, C. Wierzbicka, F. Wang, J. Li and B. Sellergren, *Sens. Actuators, B*, 2022, **368**, 132193.
32 O. Bakulina, F. K. Merkt, T. O. Knedel, C. Janiak and T. J. J. Muller, *Angew. Chem., Int. Ed.*, 2018, **57**, 17240–17244.
33 S. J. Pike, J. J. Hutchinson and C. A. Hunter, *J. Am. Chem. Soc.*, 2017, **139**, 6700–6706.
34 V. Amendola, D. Esteban-Gomez, L. Fabbrizzi and M. Licchelli, *Acc. Chem. Res.*, 2006, **39**, 343–353.
35 C. D. Geddes, *Meas. Sci. Technol.*, 2001, **12**, R53–R88.
36 S. Shinde, M. Mansour, L. Mavliutova, A. Incel, C. Wierzbicka, H. I. Abdel-Shafy and B. Sellergren, *ACS Omega*, 2022, **7**, 587–598.
37 S. Wagner, C. Zapata, W. Wan, K. Gawlitza, M. Weber and K. Rurack, *Langmuir*, 2018, **34**, 6963–6975.
38 Bindfit, **https://app.supramolecular.org/bindfit**, (accessed November 2022).
39 D. Brynn Hibbert and P. Thordarson, *Chem. Commun.*, 2016, **52**, 12792–12805.
40 P. Thordarson, *Chem. Soc. Rev.*, 2011, **40**, 1305–1323.
41 G. Wulff and K. Knorr, *Bioseparation*, 2001, **10**, 257–276.
42 R. S. Fernandes, I. M. Raimundo and M. F. Pimentel, *Colloids Surf., A*, 2019, **577**, 1–7.
43 D. J. Keddie, G. Moad, E. Rizzardo and S. H. Thang, *Macromolecules*, 2012, **45**, 5321–5342.
44 J. E. S. Schier, D. Cohen-Sacal, O. R. Larsen and R. A. Hutchinson, *Polymers*, 2017, **9**, 368.
45 S. Banerjee, *ARKIVOC (Gainesville, FL, U. S.)*, 2016, 82–110.
46 M. Divya, T. Benny, P. Christy, E. P. Aparna and K. S. Devaky, *Bioorg. Chem.*, 2017, **74**, 91–103.